General Route to Single-Crystalline SnO Nanosheets on Arbitrary Substrates

Brijesh Kumar,[†] Deuk-Hee Lee,[‡] Sang-Hyeob Kim,[§] Beelyong Yang,[#] Sunglyul Maeng,*[,||] and Sang-Woo Kim*[,†,⊥]

School of Advanced Materials Science and Engineering, Sungkyunkwan University, Suwon 440-746, Republic of Korea, Department of Electrical Engineering and Institute for Nano Science, Korea University, Seoul 136-701, Republic of Korea, IT Convergence Technology Research Laboratory, Electronics and Telecommunications Research Institute, Daejeon 305-350, Republic of Korea, Department of Advanced Nano Materials for Information Technology, Kumoh National Institute of Technology, Gumi, Gyeongbuk 730-701, Republic of Korea, Department of Electricity and Electronics Engineering, Woosuk University, Wanju, Jeonbuk 565-701, Republic of Korea, and SKKU Advanced Institute of Nanotechnology (SAINT) and Center for Human Interface Nanotechnology (HINT), Sungkyunkwan University, Suwon 440-746, Republic of Korea

Received: February 24, 2010; Revised Manuscript Received: April 25, 2010

Novel pure tin monoxide (SnO) nanosheets for use in future functional nanoscale devices were produced on indium tin oxide/glass and SiO_2/Si substrates by a thermal chemical vapor deposition process without the use of catalysts or a vacuum system. The SnO nanosheets were grown purely on the substrates without the coexistence of other nanostructures. High-resolution transmission electron microscopy investigations revealed that the structurally uniform SnO nanosheets without planar defects that were produced had preferred growth directions of $\pm[110]$ and $\pm[\bar{1}10]$ as well as a single-crystalline tetragonal structure. This work provides a general route for the facile synthesis of single-crystalline SnO nanosheets on arbitrary substrates with single, poly, or amorphous crystal structures. In addition, the selective formation of SnO nanosheets on Pt-deposited patterned SiO_2/Si substrates was successfully accomplished.

1. Introduction

Tin dioxide (SnO_2) has been regarded as a promising functional material for the realization of gas sensors with high sensitivity, solar cells, and n-type transparent conducting electrodes.[1−3] On the other hand, the material properties and device applications of tin monoxide (SnO) have rarely been investigated. Recent studies have shown that undoped SnO thin films demonstrate p-type conductivity due to naturally formed tin (Sn) vacancies, in contrast to the unintentional n-type transport behavior of undoped SnO_2.[4−6] This is extremely interesting because most metal oxides with a wide band gap show n-type conductivity.[7] However, some metal oxides, such as copper oxide and nickel oxide, also possess p-type conductivity. The fabrication of energetically stable SnO with high p-type conductivity can lead to the realization of tin oxide based p−n ($SnO-SnO_2$) junctions.

Low-dimensional metal oxide nanostructures with a well-controlled size and morphology have attracted attention due to their unique applications in electronic, optoelectronic, and spintronic devices.[8−10] Recently, one-dimensional (1D) semiconducting metal oxide nanomaterials, such as ZnO-, SnO_2-, TiO_2-, and In_2O_3-based nanowires, nanobelts, nanorods, and nanotips, have been extensively investigated.[11−15] In contrast, compared to 1D nanostructures, two-dimensional (2D) metal oxide semiconductor nanostructures have not been explored in detail and require further investigation due to difficulties in controlling nucleation and growth. Recently, 2D nanostructures, such as nanosheets,[16] nanoplates,[17] and nanowalls,[18,19] have become major topics of nanoscience and nanotechnology research. Due to the high surface-to-volume ratios of 2D nanostructures, their potential for applications in sensors for chemical and biological species, photovoltaic devices, and energy-storage devices is high.[20] Here, we report the catalyst-free and vacuum-free synthesis and characterization of single-crystalline SnO nanosheets, which have a novel nanostructural form, on indium tin oxide (ITO)-coated glass and SiO_2/Si(001) substrates using thermal chemical vapor deposition (CVD) that is regarded as one of the easiest methods for the realization of high-quality metal oxide low-dimensional nanostructures. The SnO nanosheets were grown purely on the substrates without the coexistence of other nanostructures, such as nanowires, nanobelts, and nanodisks. This work provides a general route for the facile synthesis of single-crystalline SnO nanosheets on arbitrary substrates with single, poly, or amorphous crystal structures.

2. Experimental Section

SnO nanosheets were synthesized using a thermal CVD process in a horizontal two-zone tube furnace system. A horizontal quartz tube (inner diameter = 20 mm, length = 100 cm) was mounted inside the furnace, and the second heating zone was located 40 cm downstream of the center of the first heating zone. SnO powders (99.99% purity) were loaded at the center of the first heating zone in an alumina boat. ITO/glass and SiO_2/Si(001) substrates were loaded on the quartz plate at the center of the second heating zone. At atmospheric pressure

* To whom correspondence should be addressed. E-mail: kimsw1@skku.edu (S.-W.K.), sunglyulm@gmail.com (S.M.).
† School of Advanced Materials Science and Engineering, Sungkyunkwan University.
‡ Korea University.
§ Electronics and Telecommunications Research Institute.
# Kumoh National Institute of Technology.
|| Woosuk University.
⊥ SAINT and HINT, Sungkyunkwan University.

10.1021/jp101682v
Published on Web 06/08/2010

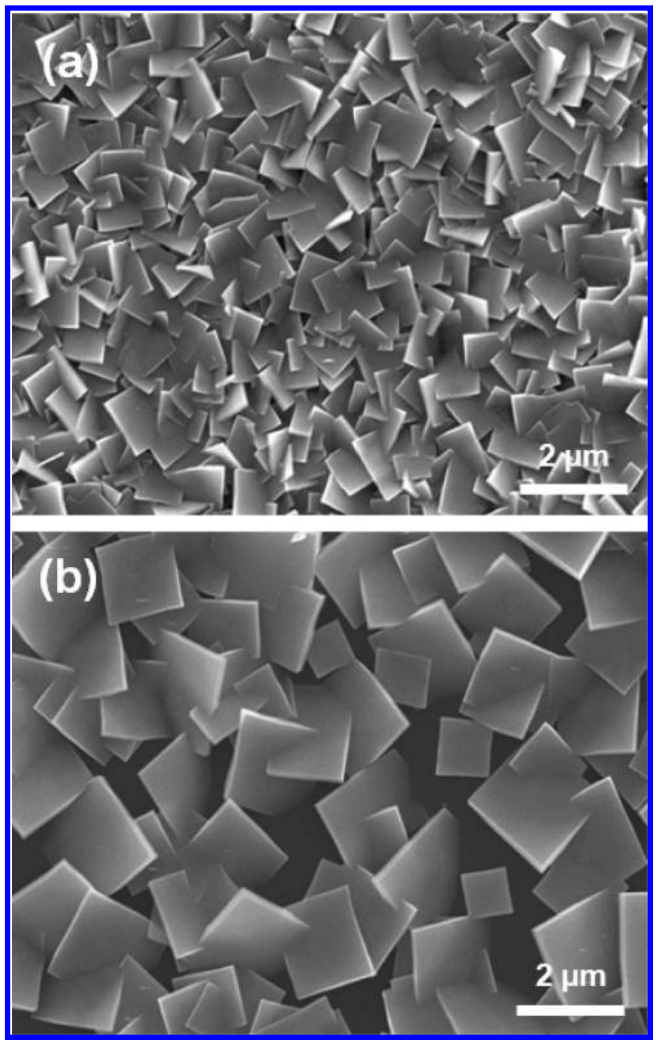

Figure 1. FE-SEM images of the as-prepared SnO nanosheets grown (a) on an ITO/glass substrate and (b) on a SiO_2/Si substrate.

and in equilibrium with the Ar carrier gas flow at 1000 sccm (standard cubic centimeters per minute), the quartz tube was heated for 180 min and held at the final temperature for 30 min (the first zone at 1000 °C and the second zone at 500 °C). After the furnace was cooled to room temperature, the grown samples were taken out of the chamber for further investigations.

The general morphology of the as-synthesized SnO nanosheets was investigated using field emission scanning electron microscopy (FE-SEM, JEOL JSM-6500F). A high-resolution transmission electron microscope (HRTEM, FE-TEM FEI TM G2 F30) was used to investigate the growth direction of the nanosheets. X-ray diffraction (XRD, Rigaku D/MAX-2500) data were collected using a standard diffractometer with Cu Kα radiation in the $\theta-2\theta$ configuration. To achieve Pt- or Au-deposited SiO_2/Si(001) substrates for the realization of selective formation of SnO nanosheets, either Pt or Au layers with a thickness of 100 nm were deposited by e-beam evaporation.

3. Results and Discussion

The plan-view FE-SEM images in Figure 1 show the general morphologies of SnO nanosheets grown on ITO/glass and SiO_2/Si substrates for 30 min at 500 °C. Compared with nanosheets grown on ITO/glass substrates, which are very dense and distributed over the entire substrate surface, as shown in Figure 1a, the SnO nanosheets on SiO_2/Si substrates are less dense, as shown in Figure 1b. Interestingly, it was found that rectangularly

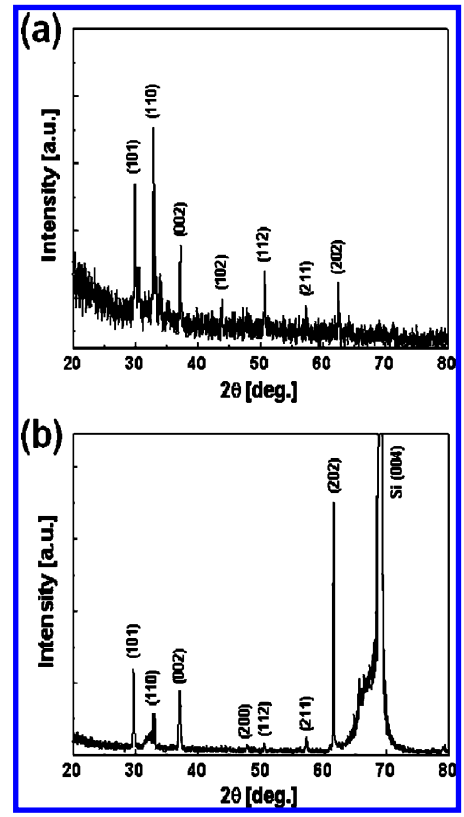

Figure 2. XRD patterns of the SnO nanosheets grown on the (a) ITO/glass substrate and on the (b) SiO_2/Si substrate.

shaped SnO nanosheets grew uniformly irrespective of the substrate material, including ITO-coated glass, bare glass, SiO_2/Si(001), and bare Si(001) substrates. In addition, the density of the grown nanosheets depends on the substrate, and the nanosheets with a higher density grown on ITO/glass substrates are smaller compared with the nanosheets grown on SiO_2/Si substrates. The nanosheets on ITO/glass substrates had lateral dimensions of $0.3-1.2$ μm and thicknesses less than 100 nm, whereas the nanosheets on SiO_2/Si substrates had lateral dimensions of $1-2$ μm and thicknesses less than 200 nm. This implies that the nucleation of SnO for nanosheet formation on an ITO surface is more effective than on the SiO_2 surface. The higher nucleation of the SnO nanosheets on ITO could be due to the presence of a large number of Sn vacancies in the ITO/glass substrate.

Figure 2 shows XRD patterns of the SnO nanosheets on ITO/glass and SiO_2/Si substrates. All of the diffraction peaks can be indexed to a tetragonal SnO structure with lattice constants of $a = 3.796$ Å and $c = 4.816$ Å. The a and b axes are equivalent, but not the c axis.[21] No diffraction peaks corresponding to metal Sn or other phases, such as SnO_2, Sn_2O_3, and Sn_3O_4, were observed.

Figure 3 shows TEM images and fast Fourier transformation (FFT) patterns of individual nanosheets physically separated from the ITO/glass and SiO_2/Si substrates and their corresponding bright-field TEM images. Figure 3a,c shows their typical rectangular morphology. Detailed structural analyses of individual nanosheets were carried out using HRTEM and FFT. The HRTEM images shown in Figure 3b,d along with the corresponding FFT patterns in the insets taken from the single nanosheet reveal that the nanosheets grown on both substrates are a single-crystalline phase with a tetragonal structure. FFT analyses indicate that the HRTEM images were taken along the [001] zone axis. Additionally, the HRTEM images show

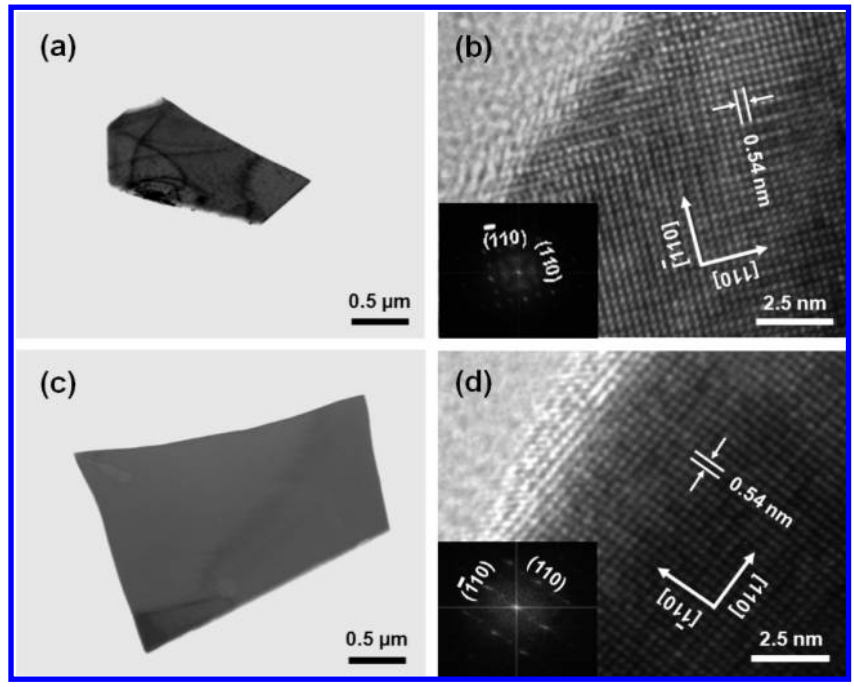

Figure 3. (a) Low-magnification bright-field TEM image and (b) HRTEM image of an individual SnO nanosheet grown on the ITO/glass substrate. The inset shows an FFT pattern of the HRTEM image shown in (a). (c) Low-magnification bright-field TEM image and (d) HRTEM image of an individual SnO nanosheet grown on the SiO_2/Si substrate. The inset shows an FFT pattern of the HRTEM image shown in (c).

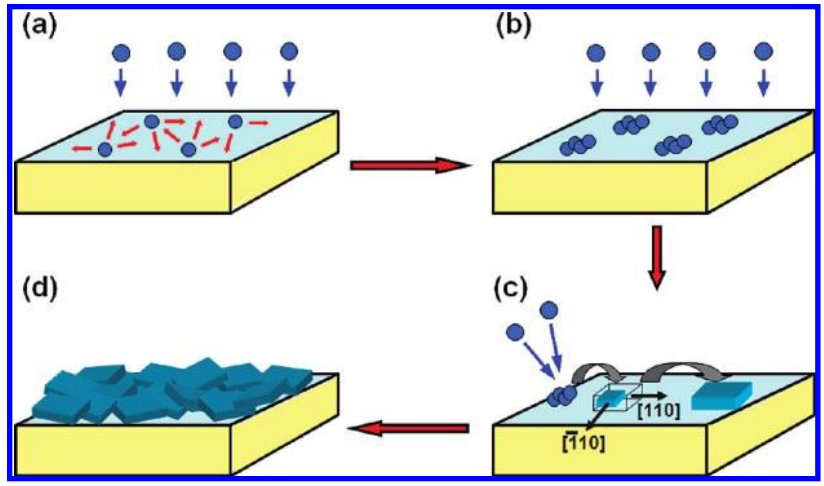

Figure 4. Schematic drawing showing the growth mechanism of the SnO nanosheets: (a) SnO vapors are dropped and diffuse onto the substrate surface, (b) SnO is nucleated and grown on the energetically favorable sites onto the substrates by a continuous supply of SnO vapors during growth, (c) SnO crystals formed by a tetragonal structure on the substrate surface are laminated successively by a continuous supply of SnO vapors due to the predominant growth of SnO along the [110] and [$\bar{1}$10] crystal directions, and (d) successive formation of SnO nanosheets with a tetragonal structure.

that the as-synthesized rectangular SnO nanosheets on both substrates are structurally uniform and free from planar defects. Furthermore, the lattice spacing of the (110) atomic planes was calculated to be 0.54 nm. On the basis of the results obtained from the HRTEM and FFT measurements, it is concluded that the preferred growth directions of the SnO nanosheets are ±[110] and ±[$\bar{1}$10] and that the nanosheets consist of a single-crystalline tetragonal structure.

Dai et al. reported the fabrication and characterization of SnO nanoscale diskettes with a tetragonal structure using thermal CVD.[21] They suggested that the formation of the SnO single crystals with a diskette shape is mainly due to the growth velocities of the SnO diskette along the [100] and [010] crystal directions, which are faster than those along the [110] and [$\bar{1}$10] crystal directions. Considering their rationale, it is also suggested that the formation of our SnO nanocrystals with a rectangular shape is mainly due to the predominant growth behavior of SnO along the [110] and [$\bar{1}$10] crystal directions. Therefore, the size of the SnO nanosheets can be controlled by varying the growth time. Large-sized nanosheets can be prepared by increasing the growth time. It is due to the preferred growth directions of ±[110] and ±[$\bar{1}$10]. Smaller-sized and thin nanosheets also can be prepared by decreasing the growth time. Further work on growth conditions to obtain larger and thinner nanosheets will be reported in the near future.

Figure 4 is a schematic drawing showing the growth mechanism of the SnO nanosheets. In general, nanostructure formation depends on vapor−solid (VS)[22] or vapor−liquid−solid (VLS)[23,24] solutions in a thermal CVD process. During the growth, SnO vapors generated at the first zone by heating at 1000 °C are transferred with the Ar carrier gas to the substrates (located at the second zone) maintained at the low temperature

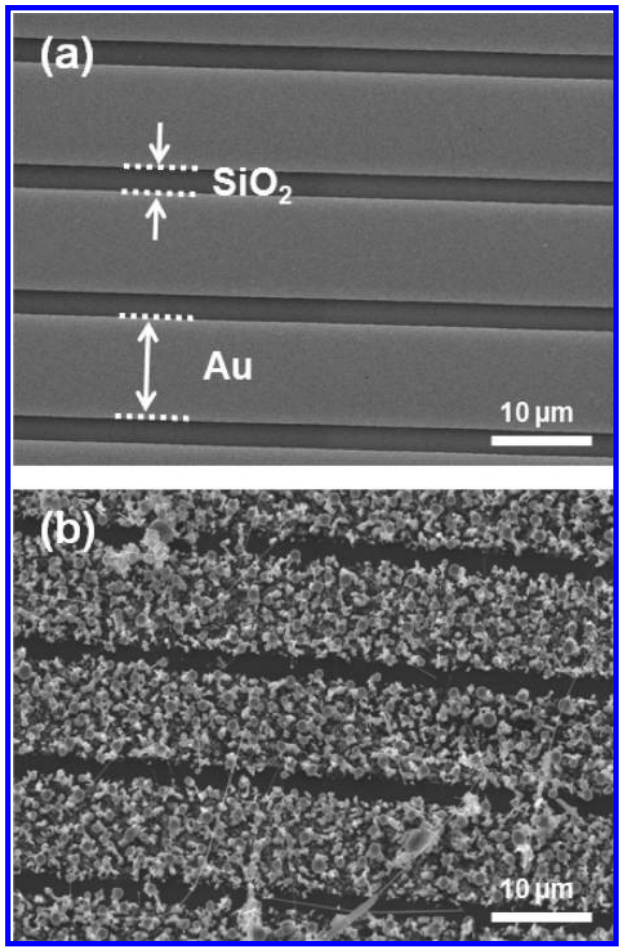

Figure 5. (a) FE-SEM image showing the Au-deposited SiO_2/Si substrate with an interdistance of about 1.8 μm between Au-deposited lines. (b) FE-SEM image revealing the surface morphology of the sample shown in (a) after SnO growth under the same growth conditions used for the fabrication of the SnO nanosheets shown in Figure 1.

of 500 °C. SnO is nucleated and grown on the energetically favorable sites onto the substrates by the continuous supply of SnO vapors during the growth, which indicates a typical VS process. SnO is laminated continuously while maintaining strong coherence of the SnO phase, resulting in the formation of SnO nanosheets. Namely, the formation of SnO nanosheets with a large (001) surface is possibly governed by the SnO tetragonal crystal structure and the preferred [110] and [$\bar{1}$10] growth directions.

A self-catalytic VLS growth process may be another possible mechanism responsible for the formation of the nanosheets because metallic Sn can easily react with oxygen, resulting in SnO formation and phase transformation. In this regard, we could not completely rule out the possibility of a self-catalytic VLS nucleation process. However, Sn-related peaks are not observed in the XRD results. Moreover, the Sn phase is unstable because an oxygen-free state in the quartz tube is not possible in the atmospheric pressure growth process used in this work without applying vacuum. Thus, it can be concluded that the formation of the SnO nanosheets mainly originates from a typical VS process.

To further clarify the mechanism of formation of the SnO nanosheets, Au-deposited (100 nm) patterned SiO_2/Si substrates were prepared, as shown in Figure 5a. The growth of SnO was carried out under the same growth conditions used for the fabrication of the nanosheets, as shown in Figure 1. Figure 5b shows an FE-SEM image revealing the surface morphology of the Au-deposited patterned SiO_2/Si substrate after SnO growth where the interdistance of the Au-deposited line patterns is about 1.8 μm. Interestingly, no nanostructures are observed on the SiO_2 layer in the close vicinity of the Au-patterned areas, whereas various nanostructures, such as ball-shaped nano- and microparticles, nanowires, and nanorods, formed randomly on the Au-patterned areas. On the other hand, dense SnO nanosheets formed on the planar SiO_2 surface far away from the Au-patterned area (not shown here). The existence of a so-called "depletion zone", where nothing grows between Au patterns, may arise due to the temperature gradient. This temperature gradient is the cause of the heat conducting nature of Au deposited on the SiO_2 surface. As a result, the sticking coefficient of SnO on Au is high, whereas it is low on the SiO_2 surface. Therefore, the preferred migration of SnO from SiO_2 to Au forms the depletion zone. The formation of a depletion zone indicates that transported SnO vapors adsorb directly and diffuse to the Au-patterned areas, leading to a preferred reaction with Au atoms rather than the bare SiO_2 surface areas between Au patterns. Thus, we suggest that the formation of SnO-based nanostructures, such as ball-shaped nano- and microparticles, nanowires, and nanobelts, on the Au-patterned areas is due to a VLS mechanism by the preferential eutectic reaction of Sn with Au atoms.

On the basis of the phenomena discussed above, we carried out selective growth of SnO nanosheets using Pt-deposited (100 nm) patterned SiO_2/Si substrates. Figure 6a,b shows typical FE-SEM images of SnO nanoplates grown on the Pt-deposited SiO_2/Si substrate with ring patterns. Unlike the results in Figure 5, SnO nanosheets were grown on bare SiO_2/Si substrates on the center of the SiO_2 surface (marked [A] in Figure 6b), as shown in Figure 6c. This indicates that a large number of nucleation sites on the SiO_2 surface area surrounded by the Pt pattern were generated. However, SnO nanoplates were hardly observed on the bare SiO_2 layer in the close vicinity of the Pt-deposited patterns (marked [B] in Figure 6b). Nanosized particles with a dramatically high density as well as nanorods formed on the Pt surfaces (marked [C] in Figure 6b) instead of nanosheets, as shown in Figure 6d. Thus, it is suggested that the formation of the dense SnO-based nanoparticles as well as nanorods on Pt is due to a VLS process although the eutectic reaction between Sn and Pt is less effective than that between Sn and Au.

Two depletion zones with widths of about 0.8 μm were found in between the Pt deposited ring on SiO_2. The depletion zone widths are smaller than the widths observed in the case of Au deposited on SiO_2 due to greater separation of the Pt deposited ring on SiO_2 than that of Au on SiO_2. If the separation of the Pt deposited ring on SiO_2 is reduced, the depletion zone will be similarly sized as the Au deposited ring. The depletion zone [B] widths were found to be almost identical between the outer ring-shaped Pt patterns, as shown in Figure 6e. The existence of the depletion zone indicates that SnO vapors prefer to form SnO on the Pt-patterned area rather than on the SiO_2 surface near the Pt pattern. Taking the growth temperature of 500 °C into account, a large number of SnO vapors or supercold liquid SnO droplets[20] can exceed the activation barrier for diffusion. This enhances the maximum diffusion length of SnO vapors from the SiO_2 surface in the close vicinity of Pt to the Pt-deposited patterned areas due to the higher sticking coefficient of Pt causing the VLS process on the Pt-deposited areas. On the other hand, SnO vapors that do not diffuse toward the Pt-deposited areas due to being out of range of the temperature gradient region can form SnO nuclei on the SiO_2 surface outside

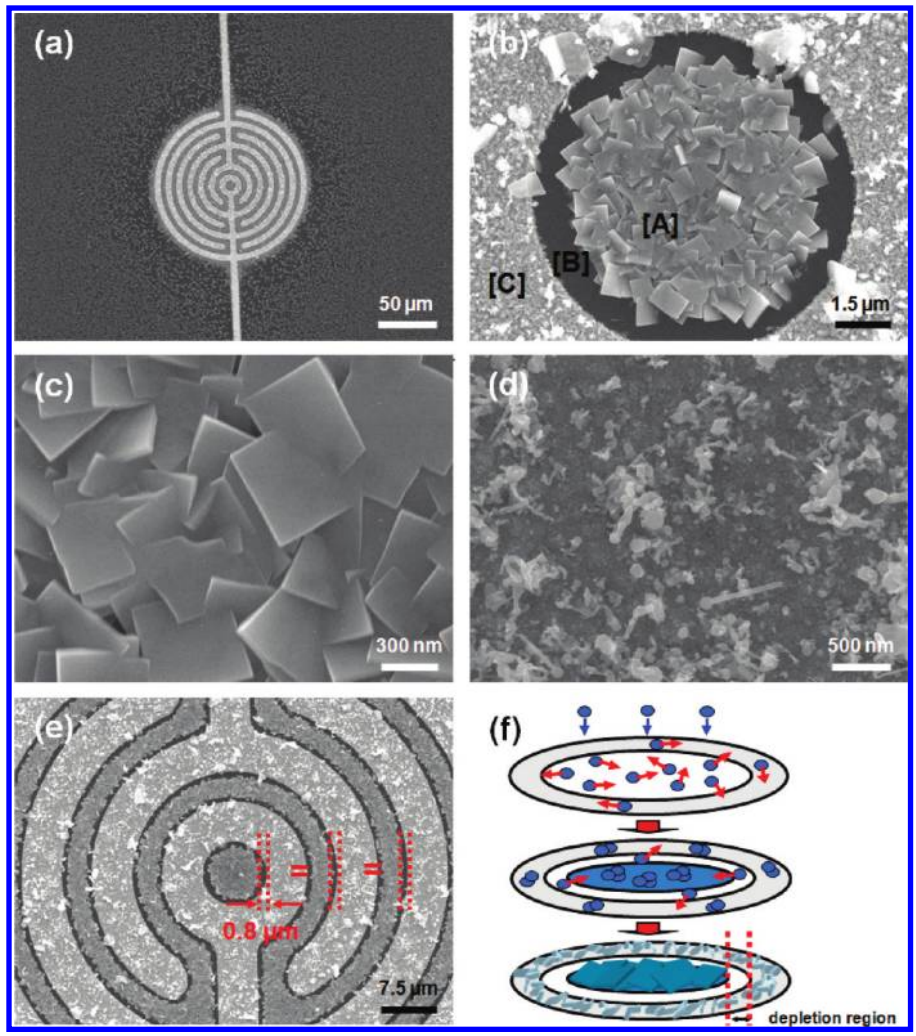

Figure 6. FE-SEM images showing surface morphologies of the sample obtained after SnO growth under the same growth conditions: (a) typical FE-SEM image of the SnO nanosheets grown on the Pt-deposited SiO_2/Si substrate with ring-shaped Pt patterns, (b) magnified FE-SEM image revealing the central part of a ring-shaped Pt pattern after SnO growth (the area marked as [A] is the center area of the SiO_2 surface with no Pt deposition, [B] is the depletion zone, and the area marked as [C] is the Pt-deposited area), (c) densely formed SnO nanosheets in the [A] area, (d) surface morphology of the Pt-deposited [C] area after growth, and (e) FE-SEM image clearly indicating that the depletion zone widths between ring-shaped Pt patterns are around 0.8 μm. (f) Schematic showing the formation mechanism of the depletion region.

the depletion region, resulting in the formation of SnO nanosheets with a tetragonal structure by continuous lamination.

4. Conclusions

In summary, we investigated the catalyst-free synthesis and characterization of pure SnO nanosheets with a single-crystalline tetragonal structure on ITO/glass and SiO_2/Si substrates using a vacuum-free thermal CVD process. The structurally uniform SnO nanosheets that were produced were confirmed via HRTEM and FFT studies to have no planar defects and to have preferred growth directions of $\pm[110]$ and $\pm[\bar{1}10]$ as well as a single-crystalline tetragonal structure. In addition, the selective formation of SnO nanosheets on Pt-deposited patterned SiO_2/Si substrates was successfully accomplished. The facile synthesis and selective formation of novel SnO nanosheets on arbitrary substrates are extremely interesting and important both for fundamental investigations of new nanostructures and for the fabrication of new functional nanoscale devices.

Acknowledgment. B.K. and D.-H.L. contributed equally to this work. This research was supported by the Conversing Research Center Program through the National Research Foundation of Korea (NRF) funded by the Ministry of Education, Science and Technology (2009-0082293) and by the Basic Science Research Program through the NRF funded by the Ministry of Education, Science and Technology (2010-0015035 and 2009-0077682). The work by S.M. was also supported by Woosuk University and the RIC program of MKE in Woosuk University.

References and Notes

(1) Xue, X.; Chen, Z.; Ma, C.; Xing, L.; Chen, Y.; Wang, Y.; Wang, T. One-Step Synthesis and Gas-Sensing Characteristics of Uniformly Loaded Pt@SnO_2 Nanorods. *J. Phys. Chem. C* **2010**, *114*, 3968–3972.

(2) Bergeron, B. V.; Marton, A.; Oskam, G.; Meyer, G. J. Dye-Sensitized SnO_2 Electrodes with Iodide and Pseudohalide Redox Mediators. *J. Phys. Chem. B* **2005**, *109*, 937–943.

(3) Harrison, P. G.; Willet, M. J. The Mechanism of Operation of Tin(IV) Oxide Carbon Monoxide Sensors. *Nature* **1988**, *332*, 337–339.

(4) Moreno, M. S.; Varela, A.; Ortero-Díaz, L. C. Cation Nonstoichiometry in Tin-Monoxide-Phase $Sn_{1-\delta}O$ with Tweed Microstructure. *Phys. Rev. B* **1997**, *56*, 5186–5192.

(5) Pan, X. Q.; Fu, L. Tin Oxide Thin Films Grown on the (1012) Sapphire Substrate. *J. Electroceram.* **2001**, *7*, 35–46.

(6) Togo, A.; Oba, F.; Tanaka, I.; Tatsumi, K. First-Principles Calculations of Native Defects in Tin Monoxide. *Phys. Rev. B* **2006**, *74*, 195128.

(7) Kawazoe, H.; Yasukawa, M.; Hyodo, H.; Kurita, M.; Yanagi, H.; Hosono, H. P-type Electrical Conduction in Transparent Thin Films of $CuAlO_2$. *Nature* **1997**, *389*, 939–942.

(8) Jonas, J.; Lisa, K.; Svensson, P. T.; Thomas, M.; Brent, W.; Knut, D.; Lars, S.; Werner, S. Structural Properties of ⟨111⟩ B -Oriented III-V Nanowires. *Nat. Mater.* **2006**, *5*, 574–580.

(9) Chueh, Y.-L.; Hsieh, C.-H.; Chang, M.-T.; Chou, L.-J.; Lao, C. S.; Song, J. H.; Gan, J.-Y.; Wang, Z. L. RuO_2 Nanowires and RuO_2/TiO_2 Core/Shell Nanowires: From Synthesis to Mechanical, Optical, Electrical, and Photoconductive Properties. *Adv. Mater.* **2007**, *19*, 143–149.

(10) Zhang, M.; Zuo, G.; Zong, Z.; Chen, H.; He, Z.; Yang, C.; Li, D.; Zou, G. Self-Assembly from the Branch Pattern to Parallel Wire Array in Electrodeposition. *Appl. Phys. Lett.* **2006**, *88*, 203106.

(11) Huang, M. H.; Mao, S.; Feick, H.; Yan, H.; Wu, Y.; King, H.; Weber, E.; Russo, R.; Yong, P. Room-Temperature Ultraviolet Nanowire Nanolasers. *Science* **2001**, *292*, 1897–1899.

(12) Xu, S.; Wei, Y.; Kirkham, M.; Liu, J.; Mai, W.; Davidovic, D.; Snyder, R. L.; Wang, Z. L. Patterned Growth of Vertically Aligned ZnO Nanowire Arrays on Inorganic Substrates at Low Temperature without Catalyst. *J. Am. Chem. Soc.* **2008**, *130*, 14958–14959.

(13) Chen, Y. J.; Li, Q. H.; Liang, Y. X.; Wang, T. H.; Zhao, Q.; Yu, D. P. Field-Emission from Long SnO_2 Nanobelt Arrays. *Appl. Phys. Lett.* **2004**, *85*, 5682–5684.

(14) Francioso, L.; Siciliano, P. Top-Down Contact Lithography Fabrication of a TiO_2 Nanowire Array over a SiO_2 Mesa. *Nanotechnology* **2006**, *17*, 3761–3767.

(15) Singh, N.; Zhang, T.; Lee, P. S. The Temperature-Controlled Growth of In_2O_3 Nanowires, Nanotowers and Ultra-Long Layered Nanorods. *Nanotechnology* **2009**, *20*, 195605.

(16) Fu, M.; Zhou, J.; Xiao, Q.; Li, B.; Zong, R.; Chen, W.; Zhang, J. ZnO Nanosheets with Ordered Pore Periodicity via Colloidal Crystal Template Assisted Electrochemical Deposition. *Adv. Mater.* **2006**, *18*, 1001–1004.

(17) Xu, L.; Zhan, J.; Hu, J.; Bando, Y.; Yuan, X.; Sekiguchi, T.; Mitome, M.; Goldberg, D. High-Yield Synthesis of Rhombohedral Boron Nitride Triangular Nanoplates. *Adv. Mater.* **2007**, *19*, 2141–2144.

(18) Kim, S.-W.; Fujita, S.; Yi, M.-S.; Yoon, D. H. Catalyst-Free Synthesis of ZnO Nanowall Networks on Si_3N_4/Si Substrates by Metalorganic Chemical Vapor Deposition. *Appl. Phys. Lett.* **2006**, *88*, 253114.

(19) Kim, S.-W.; Park, H.-K.; Yi, M.-S.; Park, N.-M.; Park, J.-H.; Kim, S.-H.; Maeng, S.-L.; Moon, S.-E. Epitaxial Growth of ZnO Nanowall Networks on GaN/Sapphire Substrates. *Appl. Phys. Lett.* **2007**, *90*, 033107.

(20) Ning, J.; Jiang, T.; Men, K.; Dai, Q.; Li, D.; Wei, Y.; Liu, B.; Chen, G.; Zou, B.; Zou, G. Syntheses, Characterizations, and Applications in Lithium Ion Batteries of Hierarchical SnO Nanocrystals. *J. Phys. Chem. C* **2009**, *113*, 14140–14144.

(21) Dai, Z. R.; Pan, Z. W.; Wang, Z. L. Growth and Structure Evolution of Novel Tin Oxide Diskettes. *J. Am. Chem. Soc.* **2002**, *124*, 8673–8680.

(22) Sekar, A.; Kim, S. H.; Umar, A.; Hahn, Y. B. Catalyst-Free Synthesis of ZnO Nanowires on Si by Oxidation of Zn Powders. *J. Cryst. Growth* **2005**, *277*, 471–478.

(23) Hao, Y.; Meng, G.; Wang, Z. L.; Ye, C.; Zhang, L. Periodically Twinned Nanowires and Polytypic Nanobelts of ZnS: The Role of Mass Diffusion in Vapor−Liquid−Solid Growth. *Nano Lett.* **2006**, *6*, 1650–1655.

(24) Fontcuberta, A.; Morral, I.; Arbiol, J.; Prades, J. D.; Cirera, A.; Morante, J. R. Synthesis of Silicon Nanowires with Wurtzite Crystalline Structure by Using Standard Chemical Vapor Deposition. *Adv. Mater.* **2007**, *19*, 1347.

JP101682V